

Measuring photometric redshifts using galaxy images and Deep Neural Networks

Ben Hoyle

*Universitaets-Sternwarte, Fakultaet fuer Physik, Ludwig-Maximilians Universitaet
Muenchen, Scheinerstr. 1, D-81679 Muenchen, Germany*

Excellence Cluster Universe, Boltzmannstr. 2, D-85748 Garching, Germany

Abstract

We propose a new method to estimate the photometric redshift of galaxies by using the full galaxy image in each measured band. This method draws from the latest techniques and advances in machine learning, in particular Deep Neural Networks. We pass the entire multi-band galaxy image into the machine learning architecture to obtain a redshift estimate that is competitive with the best existing standard machine learning techniques. The standard techniques estimate redshifts using post-processed features, such as magnitudes and colours, which are extracted from the galaxy images and are deemed to be salient by the user. This new method removes the user from the photometric redshift estimation pipeline. However we do note that Deep Neural Networks require many orders of magnitude more computing resources than standard machine learning architectures.

Keywords: Astronomy, Machine Learning, Cosmology

1. Introduction

To maximise the cosmological information available from current and upcoming large scale galaxy surveys, one requires robust distance estimates to many galaxies. The distances to galaxies are inferred by the distance-redshift

*Corresponding author

Email address: `hoyleb@usm.uni-muenchen.de, benhoyle1212@gmail.com` (Ben Hoyle)

relation which relates how the galaxy light is stretched due to the expansion of the Universe as it travels from the galaxy to our detectors. This stretching leads to an energy loss of the photon and a shift towards redder wavelengths, which is known as the redshift. The further away the galaxy is from us, the longer the light has been passing through the expanding Universe, and the more it becomes redshifted.

Obtaining very accurate spectroscopic redshifts, which measures the redshifted spectral absorption and emission lines, requires very long exposure times on dedicated spectrographs and is typically only performed for a small sub-sample of all galaxies. Conversely, the measurement of multi-band photometric properties of galaxies is much cheaper. The compromise is then to attempt to extract less accurate redshift information from photometrically measured properties, but applied to a much larger galaxy sample.

Photometric redshift estimates are obtained from either template fitting techniques, machine learning techniques, or some hybrid of the two for example using data augmentation [1]. The template methods are parametric techniques and are constructed from templates of the Spectral Energy Distribution of the galaxies. Some templates encode our knowledge of stellar population models which result in predictions for the evolution of galaxy magnitudes and colours. The parametric encoding of the complex stellar physics coupled with the uncertainty of the parameters of the stellar population models, combine to produce redshift estimates which are little better than many non-parametric techniques see e.g., [2, 3] for an overview of different techniques. Unlike non-parametric and machine learning techniques, the aforementioned template methods do not rely on training samples of galaxies, which must be assumed to be representative of the final sample of galaxies for which redshift estimates are required. Other template methods are generated either completely from, or in combination with, empirical data, however these templates both require tuning, and also rely upon representative training samples.

When an unbiased training sample is available, machine learning methods offer an alternative to template methods to estimate galaxy redshifts. The ‘ma-

chine architecture’ determines how to best manipulate the photometric galaxy input properties (or ‘features’) to produce a machine learning redshift. The machine attempts to learn the most effective manipulations to minimise the difference between the spectroscopic redshift and the machine learning redshift of the training sample.

The field of machine learning for photometric redshift analysis has been developing since [4] used artificial Neural Networks (aNNs). A plethora of machine learning architectures, including tree based methods, have been applied to the problem of point prediction redshift estimation [5] or to estimate the full redshift probability distribution function [6, 7, 8, 9]. Machine learning architectures have also had success in other fields of astronomy such as galaxy morphology identification, and star & quasar separation [10, 11].

The use of Deep Neural Networks (hereafter DNN) as the machine learning architecture has only recently been applied to problems in astrophysics. For example [12] taught a DNN to replicate the detailed morphological classifications obtained by the citizen scientists answering questions within the Galaxy Zoo 2 project [13] and obtained an accuracy of up to 99% on some classification questions, and [14] examined the problem of spectral classification from Sloan Digital Sky Survey [15] hereafter (SDSS) spectra.

Within the standard machine learning approach the choice of which photometric input features to train the machine architecture, from the full list of possible photometric features, is still left to the discretion of the user. The current author recently performed an analysis of ‘feature importance’ for photometric redshifts, which uses machine learning techniques to determine which of the many possible photometric features produce the most predictive power [16]. The technique described in this paper is the most extreme example of feature importance possible. We no longer need to impose our prior beliefs upon which derived photometric features produce the best redshift predictive power, or even measure the photometric properties. By passing the entire galaxy image into the Deep Neural Network (hereafter DNN) machine learning framework we completely remove the user from the photometric redshift estimation process.

Furthermore in order to use either the template or standard machine learning techniques to estimate redshifts, the magnitudes, colours, and other properties of the galaxies must be measured. The analysis presented in this paper, which uses the full image of the galaxy partially removes this requirement. However we do still currently need the galaxy to have been detected so that we can generate a postage stamp image.

The outline of the paper is as follows. In §2 we describe the galaxy images and the pre-processing steps to prepare the images for the Deep Neural Networks. We then introduce both of the machine learning architectures in §3, and present the analysis and results in §4, and conclude in §5.

2. Galaxy data and images

The galaxy data in this study are drawn from the SDSS Data Release 10 [15]. The SDSS I-III uses a 4 meter telescope at Apache Point Observatory in New Mexico and has CCD wide field photometry in 5 bands [17, 18], and an expansive spectroscopic follow up program [19] covering π steradians of the northern sky. The SDSS collaboration has obtained 2 million galaxy spectra using dual fibre-fed spectrographs. An automated photometric pipeline performs object classification to a magnitude of $r \approx 22$ and measures photometric properties of more than 100 million galaxies. The complete data sample, and many derived catalogs such as the photometric properties, and 5 band fits images are publicly available through the SDSS website¹.

We obtain 39,167 sets of images from the SDSS servers for a random selection of galaxies which are chosen to pass the following photometric selection criteria; the angular extent must be less than 30 arc seconds as measured by the ‘Exponential’ and ‘de’ Vacolours’ light profiles in the r band; and that each g, r, i, z have magnitudes greater than 0. We further select galaxies which pass the following spectroscopic selection criteria; the error on the spectroscopic redshift to

¹sdss.org

be less than 0.1 and the spectroscopic redshift must be below 2.

We choose to obtain the galaxy image fits files in the following four photometric bands; g, r, i, z . This enables a closer resemblance to the bands available in other photometric surveys, for example the Dark Energy Survey[20]. Each pixel in the fits file has a resolution of 0.396 arc seconds and contains the measured flux which has been corrected for a range of observational and instrument effects such as flat fielding and sky subtraction, in order to be suitable for astronomical analysis. We apply a further extinction correction to account for galactic dust. To perform this final correction we use the extinction corrections available from the SDSS website for each galaxy in each band, and subtract these values from each pixel in the corresponding fits files. We choose to use fits images of size 72x72 pixels, corresponding to 28.5 arc seconds on a side. We have explored the use of other image dimensions (32x32) but do not find improvement in the obtained results.

In the top row of Fig. 1 we show RGB jpeg images of three example galaxies with the following mappings $R \rightarrow g$ band magnitude, $G \rightarrow r$ band magnitude and $B \rightarrow i$ band magnitude. All pixel fluxes are converted to pixel magnitudes (more precisely Luptidues [21]) and are further rescaled across the entire layer to be integers within the range 0 to 255 for viewing purposes only. We further modify these base images to be more suitable for photometric redshift analysis by producing pixel colours from the pixel magnitudes and map pixel colours to each RGB layer pixel. We map the pixel colours $i - z$ to the R layer pixels, $r - i$ to the G layer pixels, and $g - r$ to the B layer pixels. Finally we pass the r band pixel magnitude into an additional Alpha layer to produce an RGBA image. The r band magnitude is often used in this way to act as a pivot point in machine learning. Examples of these modified images are shown in the second row of Fig. 1, but we show only the RGB values for viewing purposes.

During the analysis we scale all of the images, such that the maximum pixel value of 255 corresponds to the largest value across all training and test images in each of the RGBA layers separately. Likewise the minimum pixel value of 0 is set to be the smallest value in each layers across all images.

For a comparison with standard machine learning architectures we obtain model magnitudes measured by the SDSS photometric pipeline for each of the galaxies. To produce a fair comparison with the image analysis, we choose to use the de-reddened model magnitudes in the g, r, i, z bands and the size of the each galaxy measured by the Petrosian radius in the r band.

We randomly shuffle and subdivide the 39,167 galaxies into a training, cross-validation and test samples of size 33,167, 4,047, and 1,953. In what follows we train the machine learning architectures on the training sample. We then vary the hyper-parameters of the machine learning architecture and retrain a new model. We select which is the best trained model using the cross-validation sample. After choosing a final model, we pass the test sample through the final model to obtain machine learning redshift predictions. These redshift distributions produce an fair estimate of the ability of the machine learning architecture to predict redshifts for other galaxies which are representative of the training sample. In Fig. 2 we show the spectroscopic redshift number distribution of training (thick blue line) and test (thin orange line) galaxies used in this work in. The stepped lines represent the classification bins which have a width of 0.01 in redshift.

3. Machine Learning Architectures

In this work we utilise the latest developments in the field of machine learning by using Deep Neural Networks (hereafter DNNs). In particular we pass the entire galaxy image into the DNN to obtain a redshift estimate. As a comparison method we use a machine learning framework called boosted trees which produce the current state of the art photometric redshift estimates using standard photometric features. We describe both architectures in more detail below.

3.1. Deep Neural Networks

Major advances in many areas of machine learning have recently been produced using DNNs. DNNs are based on standard neural networks, which are

themselves inspired by the learning connections between biological neurons and synapses in the human brain. Neural networks have input layers, hidden layers and output layers. For our purposes, the input layers are the real valued photometric feature vectors that are measured for each galaxy. The output layer is the real valued floating point prediction for the redshift. The hidden layers are connected to the input layers and they combine and weight the input values to produce a new real valued number, which is then passed to the output layer. The weights of the connections between the layers are updated during the training phase in order to make the output value for each galaxy as close as possible to the spectroscopic redshift for that galaxy.

DNNs depart from these simple neural networks by constructing many hidden layers, with many multiple connected neurons per layer. DNNs can also accept images as input layers using an architecture called Convolutional Neural Networks[22], instead of vectors of real valued numbers. The Convolutional Neural Networks retain information about the physical location of pixels with respect to other pixels and are used efficiently in combination with the MAX OUT algorithm[23]. The power of DNNs comes from recent advances in how the connections between the many millions of neurons are trained. Previously the many millions of connections would quickly overfit even large training sets, and thereby loose the DNNs predictive power. One major advancement is the DROPOUT[24] technique, which ignores a random number of neurons during each training round. This effectively results in each training round learning a ‘weak model’, which are then combined to produce a final model with a lot of predictive power, and a lower chance of overfitting. Weak models have low predictive power by themselves, however the predictions of many weak models can be weighted and combined to produce models with much stronger predictive power.

To further ensure that the DNN does not overfit we apply data augmentation techniques to produce many training examples for each of the original input images. We apply random image flipping and rotations, and randomly select a sub patch of size 60x60 pixels to pass into the DNN. We do not currently apply

whitening techniques to add noise to the images, which can further help with overfitting.

We choose to use a base DNN architecture inspired by [25] that obtains state of the art results on the ImageNet dataset[26]. We modify the base DNN to accept images of dimension 4x60x60 and which produces an output layer with 94 classification bins, which correspond to redshift slices of width 0.01. We have also explored a limited range of DNN architectures. For example we find the using galaxy images of dimensions 4x32x32 reduces the performance by more than 30%, and increasing the dropout fraction from 0.4 to 0.9 we find that a dropout fraction of 0.6 produces slightly higher accuracy on the cross-validation. In future work we will provide a more detailed analysis of the effect of varying the hyper-parameter choices for the DNN architecture. We describe the full DNN architecture in more detail in the appendix but note here than it contains some 23 layers. In this work we use the package GRAPHLAB[27] as the main tool for building and training DNNs.

We show an illustration of the ImageNet inspired DNN with Convolutional Neural Network layers in the third row of Fig. 1 which is an altered version of an image found on <http://deeplearning.net/tutorial/lenet.html>. The modified galaxy images (second row panels) are passed into the ImageNet DNN (third row) to predict the galaxy redshift bin (final row) in a classification analysis. We choose to use an output layer consisting of 94 classification bins each corresponding to a redshift of width 0.01. Fig.2 shows the number of training and test examples per classification bin.

3.2. Tree methods

Once a galaxy has been observed and its photometric properties measured, it can be placed along with other galaxies into a high dimensional scatter diagram in which each dimension corresponding to a chosen input feature. Decision trees are machine learning architectures which subdivide this high dimensional space into high dimensional boxes. Each new split, or box, is chosen during the training phase to maximise the similarity of the spectroscopic redshifts for

all galaxies which fall within the same box. Once the space has been suitably subdivided the training ends and each box is assigned a redshift estimate which is the mean value of all remaining galaxies within the box. Test data is then placed into the high dimensional space, and the machine learning redshift estimate is assigned to the test data from the value of the hyper-box which contains it.

One may think of each individual decision tree, or configuration of hyper-boxes, as learning a weak model, and the power of tree based methods come from combining the results of many weak models to produce a final model with strong predictive power and a low chance of overfitting. There exist many techniques to choose how the individual trees should be grown, and how the trees should be combined, one of which is called Adaptive boosting, or **ADABOOST**[28, 29]. **ADABOOST** has recently been shown to provide the most accurate galaxy redshift estimates when compared with many other machine learning technologies [30]. The power of **ADABOOST** is due to the algorithm preferentially attempting to learn a good model, for those training examples with the worst performance in the previous training round.

The hyper-parameters of the scikit-learn [31] implementation of **ADABOOST** with regression trees are the number of trees combined to make the final model, the minimum number of training examples in the final hyper-boxes, the loss function, and the learning rate. We explore the full range of loss functions and other hyper-parameters within the scikit-learn implementation of **ADABOOST**. For more details on combining trees with **ADABOOST** and for further descriptions of the hyper-parameters, we refer the reader to [32]. In what follows we refer to this standard machine learning architecture using the magnitudes, colours and a r band Petrosian radius as ‘AdaBoost’

4. Results

We train both of the machine learning architectures (hereafter **MLA**) on the same sample of training galaxies, and determine how well each **MLA** has been trained by passing the cross-validation sample through the learnt machine. For

DNNs we use the full galaxy image as an input, and for AdaBoost we use the measured magnitudes, colours and radii. The output of AdaBoost is the real valued number z_{ML} , that corresponds to the photometric redshift. The output of the DNN is the redshift bin that the classified galaxy is most likely to have. The DNN randomly extracts a sub image of size 4x60x60 from the original image of size 4x72x72 and therefore can produce a different redshift prediction for each random sampling of the same image. We therefore pass each galaxy image into the final DNN one hundred times to produce a redshift classification distribution, which we then convert to a redshift vector. We calculate the mean and standard deviation of this redshift vector and label the mean redshift for this galaxy as z_{ML} . We note that if we choose to use the median instead of the mean as the redshift estimate, the final statistics vary very little.

We construct the residual vector $\Delta_z = z_{ML} - z_{spec}$ which is the difference between the machine learning redshift and the spectroscopic redshift. We measure the following metrics: $\mu, \sigma_{68}, \sigma_{95}$, corresponding to the median value of Δ_z , and the values corresponding to the 68% and 95% spread of Δ_z , and we additionally measure the ‘outlier rate’ defined as fraction of galaxies for which $|\Delta_z/(1 + z_{spec})| > 0.15$. If the residual distribution were described well by a Gaussian distribution, the choice of σ_{68} would correspond to the standard deviation, and μ would be equivalent to the mean. However most photometric redshift residual distributions have longer tails and are more peaked than a Gaussian distribution and therefore the standard deviation is not representative of the dispersion of the data.

For AdaBoost we randomly explore the hyper-parameter space 500 times and select the trained machine with the lowest value of σ_{68} as measured on the cross-validation set. Similarly, we select the final DNN from the handful of models that we explored, to be the model with the lowest value of σ_{68} as measured on the cross-validation set.

After deciding upon a final model for both MLAs we pass the sample of test galaxies, which is not used during training or model selection phase, through each MLA to obtain a final set of machine learning photometric redshifts. This

represents an unbiased estimate of the ability of the MLAs to produce redshift estimates for other galaxies, however these galaxies must be similar to, or representative of, the training sample. We again construct the residual redshift vector and measure the same statistics as before.

We present the results of the MLAs in Fig. 3. The left-hand panel shows a scatter plot of the DNN and AdaBoost redshift estimates against the spectroscopic redshift for each galaxy. The right-hand panel shows histograms of the redshift residuals. We show the results using the DNNs by the orange circles and solid lines, and the AdaBoost results by the blue stars symbols and dotted lines. The dark grey solid line shows the line of equality in the left-hand panel, and the line described by $\Delta_z = 0$ in the right-hand panel. We show the values of each of the measured statistics in Table 1. We note that the value of μ and σ_{68} for the DNNs are just very comparable to the those values obtained from AdaBoost and note that we do not expect this difference to be highly significant given the sample sizes. We find that the outlier fraction is larger by 24% for the DNNs (1.89%) compared with AdaBoost (1.52%) which may be an artefact of sample variance caused by the low number of test galaxies, or by the discreet redshift classification bins of the DNNs, compared with the continuous redshift estimate produced by the regression analysis with AdaBoost.

5. Discussion and conclusions

Robust photometric redshift estimates are a critical component of maximising the cosmological information content available from current and future photometric galaxy surveys. Indeed, recent work [9] shows how the mis-estimation of the galaxy redshift distribution for a sample of galaxies produces biases in many correlation function analyses.

In this work we propose a completely new method to obtain photometric galaxy redshift estimates by passing the full galaxy imaging into the photometric redshift estimator. We draw upon the latest techniques and architectures from the machine learning community, and use Deep Neural Networks (hereafter

DNNs) in a redshift classification analysis. To compare our results with standard machine learning photometric redshift analysis, we train a machine architecture called Decision Trees which are combined with the AdaBoost[28, 29] routine, and has recently been shown to produce state of the art photometric redshift estimates when using standard input features such as magnitudes, colors and radii [30].

The choice of which photometric standard input features to train the machine architectures, is left to the discretion of the user. However the current author recently performed an analysis of feature importance for photometric redshifts, which uses other machine learning techniques to determine which of the possible photometric quantities produce the most predictive power [16]. In order to perform a comparison between using the full image of the galaxy, and a standard analysis of derived galaxy properties, we choose to use the deredened model magnitudes in the bands g, r, i, z and the angular extent of the galaxy as measured by Petrosian radius in the r band. These choices are made for maximal comparison with other current and future photometric surveys.

For the DNNs analysis we obtain r, g, i, z fits images which we pre-process to generate four layer RGBA images, with the following mapping between layers and pixel colours and pixel magnitudes; the colours $i - z \rightarrow$ R layer, $r - i \rightarrow$ G layer and $g - r \rightarrow$ B layer. Finally we map the r band pixel magnitude into Alpha layer of the RGBA image to provide a pivot point. The layers are scaled to have integer values between 0 and 255, over the entire data sample.

We download the above photometric features and images for 39,167 galaxies from the SDSS website. We divide this data into a training, cross-validation and test sample of size 33,167, 4,047, and 1,953.

We use the latest techniques from machine learning, namely Deep Neural Networks (DNNs). We choose to use a base DNN architecture inspired by [25] that obtains state of the art results on the popular ImageNet dataset[26]. We modify the base DNN to accept galaxy images of dimension 4x60x60 and which produces an output with 100 classification bins, which correspond to redshift slices of width 0.01. We explore a limited number of different DNN architectures

a choose the best model. We leave a full analysis of DNN architectures to future work and refer to the appendix for a fuller description of the DNN architecture used in this work.

We compare the results that we obtain using galaxy images and DNNs with that using galaxy colours, magnitudes and a Petrosian radius with AdaBoost. This is performed by training the DNNs and AdaBoost on the training sample and then varying the hyper-parameters of the machine learning architectures and retraining a new system. We select which is the best system using the cross-validation sample. When we have decided upon a final system, we pass the test sample through the machine learning architecture to obtain a machine learning redshift denoted z_{ML} . This redshift produces an fair estimate of the ability of the machine learning architecture to estimate redshifts for other galaxies which are representative of the training sample.

We construct the residual vector $\Delta_z = z_{ML} - z_{spec}$ which is the difference between the machine learning redshift and the spectroscopic redshift. We measure the following metrics: $\mu, \sigma_{68}, \sigma_{95}$, corresponding to the median value of Δ_z , and the values corresponding to the 68% and 95% spread of Δ_z , and we additionally measure the ‘outlier rate’ defined as fraction of galaxies for which $|\Delta_z/(1 + z_{spec})| > 0.15$.

We note that the value of μ and σ_{68} for the DNNs (0.006,0.028) are very comparable to those values obtained from AdaBoost (0.001,0.029) and some of the difference in the median value may be caused by the discreet redshift bins chosen for the DNNs, as compared with the continuous redshift estimates produced by the regression analysis with AdaBoost. We find that the outlier fraction is larger by 24% for the DNNs (1.89%) compared with AdaBoost (1.52%) which may be an artefact of sample variance caused by the low number of test galaxies.

We note that the technique described in this paper is the most extreme example of feature importance possible. We no longer need to impose our prior beliefs upon which derived photometric features produce the best redshift predictive power, or even measure these photometric features. By passing the entire galaxy image into the machine learning framework we completely remove the

user from the photometric redshift estimation process. However we note that training and obtaining predictions using DNNs requires at least five orders of magnitude more computing resources than the standard machine learning methods such as using AdaBoost. As a consequence of this it is imperative to train the DNNs using codes optimised for GPUs.

In future work we will extend this analysis to include more training and test galaxies from the SDSS and other datasets. We will also begin to explore a much larger range of DNN architectures.

Appendix: Deep Neural Network Archtitecture

In what follows we describe the DNN used in this work. We note that this DNN is a inspired by[25] and further modified to suit our input images and output redshift classifications.

First the images of size 72x72x4 are pre-processed to obtain pixel colours, which are mapped to the RGBA layers as described in the data section. We then extract random contiguous images of size 60x60x4 from the pre-processed images. These random images are passed into the first layer of the net which is a Convolution Layer (denoted by $C_{3,10}$) which itself applies a learning smoothing filter of size 3x3x4 into a new pixel value which is stored in new sub images in the the next layer. Ten such sub images are generated in this way. The next layer is a Rectified Linear Layer (R) and transforms all of the input values into output values using the function $f(x) = \max(0, x)$ and passes the transformed values to a MaxPooling Layer (MP_3) which is similar to the filtering in the C layer, but instead outputs the maximum value of the 3x3 filtered sub image into the next layer. The next layer is a Local Renormalisation Layer (RN_5) which normalised the output values by the values coming from 5 neighbouring neurons. The subsequent Layers are $C_{5,256} \rightarrow R \rightarrow MP_3 \rightarrow RN_5 \rightarrow C_{3,384} \rightarrow R \rightarrow C_{3,384} \rightarrow R \rightarrow C_{3,256} \rightarrow R, MP_3$, which is then followed by a flattening layer which converts the Convolutional type layers into flat layers such as those found in standard neural networks. The flattened layer is

MLA	μ	σ_{68}	σ_{95}	$ \Delta_z/(1 + z_{spec}) > 0.15$
DNNs	-0.006	0.028	0.104	1.89%
AdaBoost	-0.001	0.029	0.099	1.52%

Table 1: The statistics measured on each of the best machine learning architectures (MLA) are shown in the column headings, and are measured on the redshift residual distribution Δ_z of the test galaxies, which are not used during training or model selection.

then followed by a Fully Connected (F_{4096}) layer with 4096 neurons followed by R and then a Dropout Layer $D_{0.6}$ which has with a probability of 0.6 that each neuron is completely ignored during this training phase. This Dropout layer is followed by F_{4096} , R, F_{94} corresponding to the 94 redshift classes which are finally normalised and converted into class probabilities using a Softmax layer.

Acknowledgements

I would like to thank Sander Deileman and Kerstin Peach for useful discussions and Jochen Weller and Stella Seitz for proof reading and comments. The author declares no competing financial interests.

References

References

- [1] B. Hoyle, M. M. Rau, C. Bonnett, S. Seitz, J. Weller, Data augmentation for machine learning redshifts applied to SDSS galaxies, ArXiv e-prints [arXiv:1501.06759](https://arxiv.org/abs/1501.06759).
- [2] H. Hildebrandt, S. Arnouts, P. Capak, L. A. Moustakas, C. Wolf, e. a. Abdalla, PHAT: PHoto-z Accuracy Testing, Astron. & Astrophys. 523 (2010) A31. [arXiv:1008.0658](https://arxiv.org/abs/1008.0658), doi:10.1051/0004-6361/201014885.
- [3] T. e. a. Dahlen, A Critical Assessment of Photometric Redshift Methods: A CANDELS Investigation, ApJ 775 (2013) 93. [arXiv:1308.5353](https://arxiv.org/abs/1308.5353), doi:10.1088/0004-637X/775/2/93.

- [4] R. Tagliaferri, G. Longo, S. Andreon, S. Capozziello, C. Donalek, G. Giordano, Neural Networks for Photometric Redshifts Evaluation, Lecture Notes in Computer Science 2859 (2003) 226–234. [arXiv:astro-ph/0203445](https://arxiv.org/abs/astro-ph/0203445), doi:10.1007/978-3-540-45216-4_26.
- [5] e. a. Sánchez, C., Photometric redshift analysis in the Dark Energy Survey Science Verification data, MNRAS445 (2014) 1482–1506. [arXiv:1406.4407](https://arxiv.org/abs/1406.4407), doi:10.1093/mnras/stu1836.
- [6] D. W. Gerdes, A. J. Sypniewski, T. A. McKay, J. Hao, M. R. Weis, R. H. Wechsler, M. T. Busha, ArborZ: Photometric Redshifts Using Boosted Decision Trees, ApJ715 (2010) 823–832. [arXiv:0908.4085](https://arxiv.org/abs/0908.4085), doi:10.1088/0004-637X/715/2/823.
- [7] M. Carrasco Kind, R. J. Brunner, TPZ: photometric redshift PDFs and ancillary information by using prediction trees and random forests, MNRAS432 (2013) 1483–1501. [arXiv:1303.7269](https://arxiv.org/abs/1303.7269), doi:10.1093/mnras/stt574.
- [8] C. Bonnett, Using neural networks to estimate redshift distributions. An application to CFHTLenS, ArXiv e-prints [arXiv:1312.1287](https://arxiv.org/abs/1312.1287).
- [9] M. M. Rau, S. Seitz, F. Brimioule, E. Frank, O. Friedrich, D. Gruen, B. Hoyle, Accurate photometric redshift probability density estimation - method comparison and application, ArXiv e-prints [arXiv:1503.08215](https://arxiv.org/abs/1503.08215).
- [10] O. Lahav, Artificial neural networks as a tool for galaxy classification., in: V. Di Gesu, M. J. B. Duff, A. Heck, M. C. Maccarone, L. Scarsi, H. U. Zimmerman (Eds.), Data Analysis in Astronomy, 1997, pp. 43–51. [arXiv:astro-ph/9612096](https://arxiv.org/abs/astro-ph/9612096).
- [11] C. Yéche, P. Petitjean, J. Rich, E. Aubourg, N. Busca, J. . Hamilton, J. . Le Goff, I. Paris, S. Peirani, C. Pichon, E. Rollinde, M. Vargas-Magana, QSO Selection and Photometric Redshifts with Neural Networks, ArXiv e-prints [arXiv:0910.3770](https://arxiv.org/abs/0910.3770).

- [12] S. Dieleman, K. W. Willett, J. Dambre, Rotation-invariant convolutional neural networks for galaxy morphology prediction, ArXiv e-prints [arXiv:1503.07077](https://arxiv.org/abs/1503.07077).
- [13] K. W. Willett, C. J. Lintott, S. P. Bamford, K. L. Masters, et al., Galaxy Zoo 2: detailed morphological classifications for 304 122 galaxies from the Sloan Digital Sky Survey, MNRAS435 (2013) 2835–2860. [arXiv:1308.3496](https://arxiv.org/abs/1308.3496), doi:10.1093/mnras/stt1458.
- [14] P. Hála, Spectral classification using convolutional neural networks, ArXiv e-prints [arXiv:1412.8341](https://arxiv.org/abs/1412.8341).
- [15] C. P. Ahn, R. Alexandroff, C. Allende Prieto, F. Anders, S. F. Anderson, T. Anderton, B. H. Andrews, É. Aubourg, S. Bailey, F. A. Bastien, et al., The Tenth Data Release of the Sloan Digital Sky Survey: First Spectroscopic Data from the SDSS-III Apache Point Observatory Galactic Evolution Experiment, ApJS211 (2014) 17. [arXiv:1307.7735](https://arxiv.org/abs/1307.7735), doi:10.1088/0067-0049/211/2/17.
- [16] B. Hoyle, M. M. Rau, R. Zitzlau, S. Seitz, J. Weller, Feature importance for machine learning redshifts applied to SDSS galaxies, MNRAS449 (2015) 1275–1283. [arXiv:1410.4696](https://arxiv.org/abs/1410.4696), doi:10.1093/mnras/stv373.
- [17] J. E. Gunn, W. A. Siegmund, E. J. Mannery, R. E. Owen, C. L. Hull, R. F. Leger, L. N. Carey, G. R. Knapp, D. G. York, W. N. Boroski, S. M. Kent, R. H. Lupton, C. M. Rockosi, et al., The 2.5 m Telescope of the Sloan Digital Sky Survey, AJ131 (2006) 2332–2359. [arXiv:arXiv:astro-ph/0602326](https://arxiv.org/abs/arXiv:astro-ph/0602326), doi:10.1086/500975.
- [18] J. A. Smith, et al., The u'g'r'i'z' Standard-Star System, AJ123 (2002) 2121–2144. [arXiv:arXiv:astro-ph/0201143](https://arxiv.org/abs/arXiv:astro-ph/0201143), doi:10.1086/339311.
- [19] e. a. Eisenstein, D. J., SDSS-III: Massive Spectroscopic Surveys of the Distant Universe, the Milky Way, and Extra-Solar Planetary Systems, AJ142 (2011) 72. [arXiv:1101.1529](https://arxiv.org/abs/1101.1529), doi:10.1088/0004-6256/142/3/72.

[20] The Dark Energy Survey Collaboration, The Dark Energy Survey, ArXiv Astrophysics e-prints [arXiv:astro-ph/0510346](https://arxiv.org/abs/astro-ph/0510346).

[21] R. H. Lupton, J. E. Gunn, A. S. Szalay, A Modified Magnitude System that Produces Well-Behaved Magnitudes, Colors, and Errors Even for Low Signal-to-Noise Ratio Measurements, *AJ*118 (1999) 1406–1410. [arXiv:astro-ph/9903081](https://arxiv.org/abs/astro-ph/9903081), doi:10.1086/301004.

[22] Y. Lecun, Y. Bengio, Convolutional Networks for Images, Speech and Time Series, The MIT Press, 1995, pp. 255–258.

[23] I. J. Goodfellow, D. Warde-Farley, M. Mirza, A. Courville, Y. Bengio, Maxout Networks, ArXiv e-prints [arXiv:1302.4389](https://arxiv.org/abs/1302.4389).

[24] G. E. Hinton, N. Srivastava, A. Krizhevsky, I. Sutskever, R. R. Salakhutdinov, Improving neural networks by preventing co-adaptation of feature detectors, ArXiv e-prints [arXiv:1207.0580](https://arxiv.org/abs/1207.0580).

[25] A. Krizhevsky, I. Sutskever, G. E. Hinton, Imagenet classification with deep convolutional neural networks, in: F. Pereira, C. Burges, L. Bottou, K. Weinberger (Eds.), *Advances in Neural Information Processing Systems* 25, Curran Associates, Inc., 2012, pp. 1097–1105.
 URL <http://papers.nips.cc/paper/4824-imagenet-classification-with-deep-convolutional-neural-networks.pdf>

[26] O. Russakovsky, J. Deng, H. Su, J. Krause, S. Satheesh, S. Ma, Z. Huang, A. Karpathy, A. Khosla, M. Bernstein, A. C. Berg, L. Fei-Fei, ImageNet Large Scale Visual Recognition Challenge, ArXiv e-prints [arXiv:1409.0575](https://arxiv.org/abs/1409.0575).

[27] Y. Low, J. Gonzalez, A. Kyrola, D. Bickson, C. Guestrin, J. M. Hellerstein, GraphLab: A New Framework for Parallel Machine Learning, ArXiv e-prints [arXiv:1006.4990](https://arxiv.org/abs/1006.4990).

[28] Y. Freund, R. E. Schapire, A decision-theoretic generalization of on-line learning and an application to boosting, *Journal*

nal of Computer and System Sciences 55 (1) (1997) 119 – 139.
doi:<http://dx.doi.org/10.1006/jcss.1997.1504>.

URL <http://www.sciencedirect.com/science/article/pii/S002200009791504X>

[29] H. Drucker, Improving regressors using boosting techniques, in: Proceedings of the Fourteenth International Conference on Machine Learning, ICML '97, Morgan Kaufmann Publishers Inc., San Francisco, CA, USA, 1997, pp. 107–115.
URL <http://dl.acm.org/citation.cfm?id=645526.657132>

[30] B. Hoyle, M. M. Rau, K. Paech, C. Bonnett, S. Seitz, J. Weller, Anomaly detection for machine learning redshifts applied to SDSS galaxies, ArXiv e-prints [arXiv:1503.08214](https://arxiv.org/abs/1503.08214).

[31] F. Pedregosa, et al., Scikit-learn: Machine learning in python, Journal of Machine Learning Research 12 (2011) 2825–2830.

[32] T. Hastie, R. Tibshirani, J. Friedman, The Elements of Statistical Learning, Springer Series in Statistics, Springer New York Inc., New York, NY, USA, 2001.

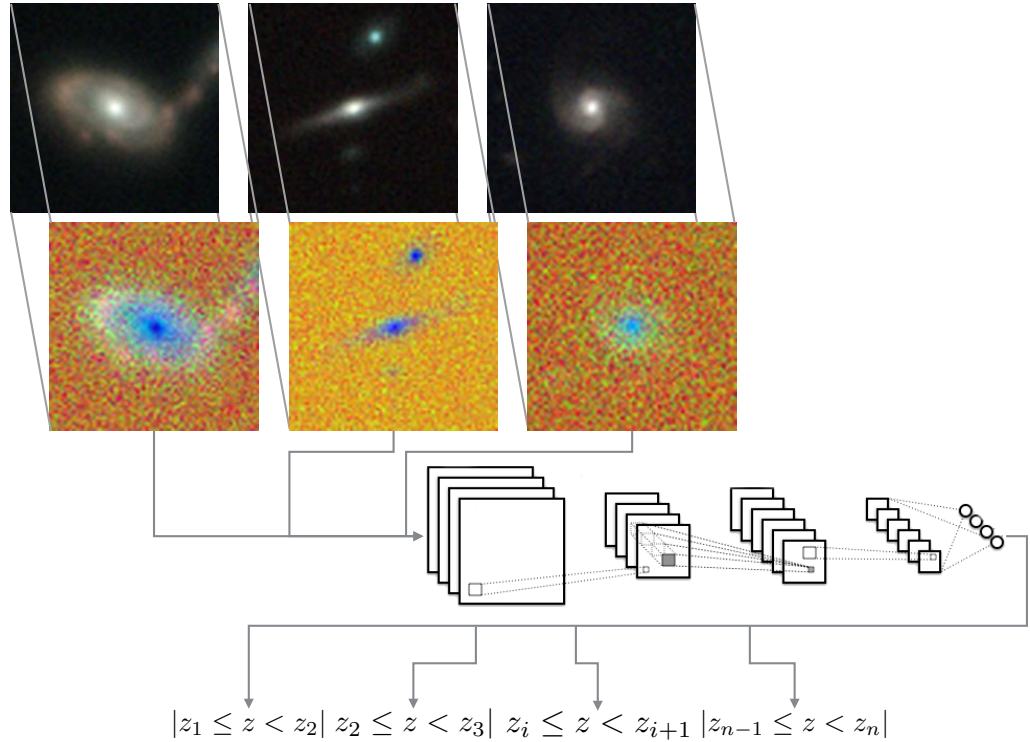


Figure 1: The experimental set up with the ImageNet inspired Deep Neural Network (DNN) with Convolutional layers. We convert the pixel fluxes (top images) to pixel magnitudes and subtract magnitudes to make pixel colours. Each colour is placed into a separate image layer (see examples in the second row). These modified images are passed into a DNN (illustrated by the third row) to predict the galaxy redshift (z) bin (bottom panel). Partial image credit in text.

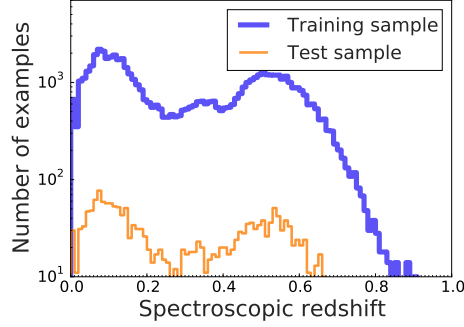


Figure 2: The redshift number distribution of training (thick blue line) and test (thin orange line) galaxies used in this work. The stepped lines represent the classification bins which are of width 0.01.

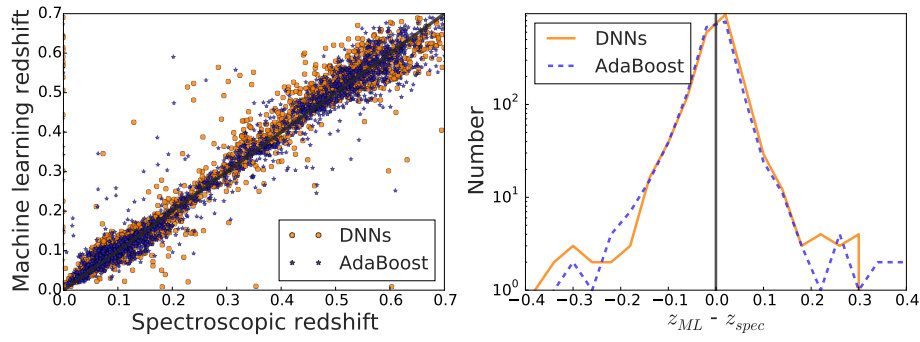


Figure 3: The left-hand panel shows the DNNs machine learning redshift estimate against the spectroscopic redshift by the orange circles, and the AdaBoost machine learning redshift estimate by the blue stars. The right-hand panel presents histograms of the redshift residuals for DNNs by the solid orange line, and AdaBoost by the blue dotted line. The dark grey solid line shows the line of equality in the left-hand panel, and the line described by $\Delta z = 0$ in the right-hand panel.